Published in final edited form as:
NMR Biomed. 2014 November ; 27(11): 1378–1386. doi:10.1002/nbm.3200.

Characterization of Diffuse Fibrosis in the Failing Human Heart via Diffusion Tensor Imaging and Quantitative Histological Validation

Osama M. Abdullah, MS[1], **Stavros G. Drakos, MD**[2,3], **Nikolaos A. Diakos, MD**[2], **Omar Wever-Pinzon, MD**[3], **Abdallah G. Kfoury, MD**[3], **Josef Stehlik, MD**[3], **Craig H. Selzman, MD**[3], **Bruce B. Reid, MD**[3], **Kim Brunisholz, MS**[3], **Divya Ratan Verma, MD**[3], **Craig Myrick, MD**[4], **Frank B. Sachse, PhD**[1,5], **Dean Y. Li, MD, PhD**[2], and **Edward W. Hsu, PhD**[1]

[1]Department of Bioengineering, University of Utah

[2]Molecular Medicine Program, University of Utah

[3]UTAH Cardiac Transplant Program (University of Utah Hospital, Intermountain Medical Center, Salt Lake Veterans Affairs Medical Center)

[4]Intermountain Donor Services

[5]Nora Eccles Harrison Cardiovascular Research and Training Institute, University of Utah

Abstract

Non-invasive imaging techniques are highly desirable as an alternative to conventional biopsy for characterizing remodeling of tissues associated with disease progression, including end-stage heart failure. Cardiac diffusion tensor imaging (DTI) has become an established method for characterizing myocardial microstructure. However, the relationships between diffuse myocardial fibrosis, which is a key biomarker for staging and treatment planning of the failing heart, and measured DTI parameters have yet to be systematically investigated. In this study, DTI was performed on left ventricular specimens collected from patients with chronic end-stage heart failure due to idiopathic dilated cardiomyopathy (n=14) and from normal donors (n=5). Scalar DTI parameters, including fractional anisotropy (FA), mean (MD), primary (D_1), secondary (D_2), and tertiary (D_3) diffusivities, were correlated to collagen content measured by digital microscopy. Compared to hearts from normal subjects, the FA in failing hearts decreased by 22%, whereas the MD, D_2 and D_3 increased by 12%, 14%, and 24% respectively ($P < 0.01$). No significant change was detected for D_1 between the two groups. Furthermore, significant correlation was observed between the DTI scalar indices and quantitative histological measurements of collagen (i.e., fibrosis). Pearson's correlation coefficient (r) between collagen content and either FA, MD, D_2, and D_3 was -0.51, 0.59, 0.56 and 0.62 ($P < 0.05$), respectively. The correlation between D_1 and collagen content was not significant ($r = 0.46$, $P = 0.05$). Computational modeling analysis indicated that the behaviors of the DTI parameters as a function of the degree of fibrosis were well explained by compartmental exchange between myocardial and collagenous tissues. Combined,

Corresponding Author: Osama M. Abdullah, Department of Bioengineering, University of Utah, 36 S Wasatch Dr., Rm 3100, Salt Lake City, Utah 84112, Phone: (1) 801-587-8357, Osama.Abdullah@utah.edu.

these findings suggest that scalar DTI parameters can be used as metrics for noninvasive assessment of diffuse fibrosis in failing hearts.

Keywords

DTI; non-ischemic heart failure; diffuse fibrosis; histological correlation; fractional anisotropy; mean diffusivity; principal diffusivities; idiopathic dilated cardiomyopathy

Introduction

End stage heart failure (HF) is a major public health problem with high mortality, morbidity and cost to the healthcare systems in the US and Europe (1,2). The disease is characterized by adverse changes in cardiac structure and function as a result of mechanical, neurohormonal, and cardiorenal factors (3). One of the main factors leading to HF is the development of pathological myocardial fibrosis. Abnormally high collagen content adversely impacts the mechanical (4) and electrical (5) behaviors of the myocardium, and has been linked to increased risk of ventricular and atrial tachyarrhythmias and sudden cardiac death (6).

Myocardial fibrosis has been classified into reparative or reactive (7). In myocardial infarction (MI), fibrotic scar forms as macroscopic patches of collagen following myocytes necrosis to protect the myocardium from rupturing, and is thus called reparative fibrosis. On the other hand, collagen that develops in the remote zone to infarcts or in non-ischemic cardiac disease (such as dilated cardiomyopathy or cardiac hypertrophy) manifests as microscopic collagen depositions in the interstitial space and is termed reactive or diffuse fibrosis. Diffuse fibrosis is known to increase ventricular stiffness and leads to pump dysfunction (7,8), and has been suggested to play a more detrimental role in structural remodeling in ischemic disease than the fibrotic scarring (9). To date, tissue biopsy and histology remain the gold-standard method for quantifying structural remodeling in HF for staging and treatment planning of the disease (10,11). However, the invasive and laborious nature of the histological procedures presents a practical limitation on the number of sites and time points that can be practically performed. Hence, non-invasive imaging techniques for quantifying myocardial diffuse fibrosis are highly desirable.

Magnetic resonance diffusion tensor imaging (MR-DTI, or DTI for short), which captures the dependence of tissue water diffusion on the molecular environment (12), has emerged as an established, non-invasive alternative to histology for characterizing myocardial tissue microstructure. Technically, DTI yields a second-rank, symmetric matrix that describes both the direction and magnitude of the diffusion anisotropy, which can in turn be used to infer the underlying tissue organization, geometry and content. For example, the direction in which diffusion is the fastest (i.e., the eigenvector of the largest diffusion tensor eigenvalue) has been found to coincide with the local fiber orientation in freshly excised (13), perfused (14), and formalin-fixed (15) myocardium. Moreover, the eigenvector of the second diffusion tensor eigenvalue has been associated with the orientation of myocardial sheet structure (16). So far, DTI has been used to characterize the structures of normal hearts in a variety of small and large animal models (17–21), in addition to humans (22,23)

Although cardiac DTI has been utilized to study cardiac pathologies of both ischemic and nonischemic origins, there is a lack of data to quantify diffuse fibrosis in disease conditions. Studies of ischemic injury reported a reduction in the degree of diffusion anisotropy coupled with an increase of water diffusivity in the infarct zone in humans, albeit no histological validation was provided (24,25). Similar DTI changes to those observed in clinical studies were reported in animal models of ischemic injury, which attributed the changes to a combination of myocytes death, fiber disarray, and the subsequent forming of fibrotic scarring as confirmed histologically (26,27). Furthermore, the ability of diffusion weighted imaging to delineate both infarct and infarct-border zones was demonstrated by correlating diffusion coefficient maps to late gadolinium enhancement images and histological collagen stain (28).

Additionally, DTI has been utilized in assessing nonischemic cardiac disease, such as dyssynchronous HF (29), hypertrophic cardiomyopathy (30), and dilated cardiomyopathy (31,32). Most studies in this category, however, focused on quantifying fiber orientation changes due to nonischemic disease (29–31). Besides changes in the fiber orientation, the diseased myocardium (e.g., hypertrophy or dilated cardiomyopathy) was reported to have decreased diffusion anisotropy (30,32) and increased water diffusivity (32). One DTI study was performed on aging animal model of dilated cardiomyopathy and qualitatively associated the scalar DTI parameters to calcium and collagen depositions in the diseased hearts (32). Although the latter changes can be associated with myocardial fibrosis, the exact relationships between myocardial diffuse fibrosis and the DTI scalar parameters remain yet to be quantitatively determined.

Beyond the empirical observations, to better understand the origin and predict the behavior of the relationship, it is also useful to explore the biophysical basis of dependence of the measured DTI indices on myocardial collagen content. Compartmental exchange models have been used to approximate the behavior of the MRI signal arising from a heterogeneous microscopic environment (33,34), which is to be expected of the fibrotic myocardium. In the so-called fast-exchange situation, water spins spend much shorter time in the compartments than the temporal-length scale of their molecular dynamics. Then the MRI parameters (e.g., relaxation rate and diffusion constants) of the aggregate system behave like the fractional volume-weighted sum of the same parameters of the individual compartments. Conversely under the slow-exchange limit, the overall MRI signal is simply the proportional superposition of the signals from the individual compartments, as if the latter are completely independent. Bi-compartmental slow exchange models have been used to describe the MRI diffusion signal, including DTI, observed in the myocardium (35,36). Although it is unclear whether the behavior of the fibrotic myocardium is better described by the fast or slow-exchange model, either mechanism provides a possible starting point to explain the role in which diffuse fibrosis contributes to the MRI signal of the diseased myocardium.

Taken together, the present study aims to quantify the relationship between the DTI parameters and diffuse fibrosis, and to explore the biophysical explanations of the relationships. While fiber orientation remodeling associated with heart diseases has been examined in previous studies (29,30), the current work focuses on the scalar DTI parameters. To reduce measurement subjectivity, histological examination of the

myocardium is performed using state-of-the-art, whole-field digital microscopy for comprehensive endocardium-to-epicardium evaluation, followed by quantitative image analysis (37). Findings of the current study are expected to be important for assessing the utility of DTI, and to pave the way for the technique to be used in eventual *in vivo* studies on HF patients.

Methods

Study Population and Specimen Collection

The study was approved by the Institutional Review Board at the University of Utah. The study group comprised 14 patients with chronic end-stage HF due to idiopathic dilated cardiomyopathy who required implantation of a left ventricular assist device (LVAD) for either bridge to heart transplantation or destination therapy in 2010. All patients met the medical policy guideline of New York Heart Association (NYHA) class IIIb/IV for HF. The control group consisted of five donors whose hearts were determined to be functionally and structurally normal but were not suitable for transplantation due to non-cardiac reasons.

Heart specimens were collected at the time of LVAD implantation by excising approximately a $1 \times 1 \times 1$ cm^3 transmural plug from the left ventricular apex. The normal hearts were collected as intact specimens, and a similar section from the left ventricular apex was obtained for histology. All specimens were fixed in 10% buffered formalin for at least 24 h prior to further examination. The average time between fixation and MR imaging was 4 ± 2 weeks. The DTI parameters were shown to remain constant 24 hours after the initial cross-linking due to formalin fixation for several weeks (38,39). Quantitative correlation between DTI and histology was performed on specimens obtained from the same heart taken few millimeters apart. Similar regions were analyzed in both HF and control groups. Sample preparation and correlation procedure followed previously published studies (37,40).

Demographic, clinical, echocardiographic, hemodynamic, and laboratory data were collected 48-72 h prior to surgery and tissue collection. The collected information from the end-stage HF patients and the normal donors are shown in Table 1. HF in the diseased group was confirmed by left ventricle ejection fraction, which was almost 4 times lower versus the normal group. All HF subjects had non-ischemic cardiomyopathies and are expected to predominantly have diffuse fibrosis.

MRI Acquisition and Analysis

MRI experiments were conducted on a Bruker 7.0 T horizontal bore MRI scanner (Bruker Biospin, Germany) interfaced with 12.0 cm-diameter actively shielded gradient insert (BGA12S) capable of producing magnetic field gradients of up to 600 mT/m. Each heart specimen was placed in a sealed container filled with susceptibility matching fluid (Fomblin, Solvay Solexis, NJ, USA). A combination of a linear volume coil (72 mm inner diameter) for signal transmission and a quadrature surface coil (25 mm inner diameter) for signal reception were used to acquire the DTI datasets.

DTI acquisition was performed using a standard multi-slice diffusion-weighted spin echo sequence with the following imaging parameters: 2000/30 ms TR/TE, 64 × 64 matrix size

with 1.5 mm in-plane resolution, 4 transverse slices, with 1.0 mm thickness. Diffusion was encoded along a set of 12 optimized gradient directions (41), using a pair of trapezoidal gradient pulses of 0.25 ms rise time, 4.00 ms duration (δ), and 10.00 ms separation (Δ), equivalent to a nominal b-value of 1500 s/mm^2. The average signal-to-noise ratio (SNR) for the non-diffusion weighted image (B0) was 80. The total scan time for each specimen was approximately 28 min.

Post-processing computation was performed using custom-codes written in Matlab (Version R2010a, Mathworks, MA) as described previously (12). Briefly, diffusion tensors were estimated on a pixel-by-pixel basis from the MR diffusion images and diagonalized to yield the 3 eigenvalues (D_1, D_2 and D_3, in sorted descending order and commonly referred to as primary, secondary, and tertiary diffusivities, respectively) and eigenvectors, which are equivalent to the speeds and principal axes of diffusion, respectively. The diffusion tensor eigenvalues were in turn used to obtain the mean diffusivity (MD) and fractional anisotropy (FA), which represent the magnitude of diffusion and degree of anisotropy, respectively, and are commonly used scalar indices for characterizing tissue microstructure (42). MD and FA were reported as averages over the entire myocardial area on all 4 image slices for each specimen. The average area of the selected regions of interest (ROIs) across all samples was 0.79 ± 0.08 cm^2 per slice (n = 19, mean ± SEM). To determine the underlying source of observed changes in the MD or FA, averages of the principal diffusivity terms D_1, D_2, and D_3 were similarly obtained.

Histology: Whole-Field Digital Microscopy

For histology, specimens were dehydrated in progressively higher concentrations of alcohol, cleared through xylene and embedded in paraffin. One representative, 4 μm-thick, section from each specimen was obtained and mounted on a glass slide. It was then evaluated on a whole-field basis spanning the entire myocardial wall (epicardium to endocardium) using a ScanScope XT digital histopathology system equipped with the ImageScope 10.0 image analysis software (Aperio Technologies, CA) as described previously (37). Quantitative histological measurements to quantify diffuse fibrosis percentage in the heart specimen were conducted using Masson's trichrome stain for collagen content evaluation. The collagen content was automatically quantified by identifying, counting and expressing the number of blue-staining pixels as a percentage of the total tissue area (37). Because of the relatively low spatial resolution of the DTI scans (1.5 mm), which was insufficient to directly visualize the interstitial content, the degree of diffuse fibrosis was approximated by the total collagen detected on the whole histological slide (endocardium to epicardium).

Statistical Analysis

Statistical analysis was performed using GraphPad Prism (Version 5.0a, GraphPad Software Inc., CA). Variables were reported as mean and standard error of the mean (SEM). All parameters measured in the current study, including both DTI and histological indices, were compared between the failing and normal control groups using a two-tailed unpaired t-tests. A *P*-value less than 0.05 was considered to be statistically significant. Correlation between DTI and histological indices was determined by evaluating the Pearson's correlation coefficients (r) for all pairings of MRI and histology parameters.

Computational Compartmental Analysis

Computational simulations were performed as a means to explain the behavior of the DTI experiment in the myocardium with varying amount of fibrosis. Monte Carlo simulations of DTI parameters that would have been measured in standard DTI experiments were conducted assuming that the diffusion signal originated from either fast or slow compartmental exchange between myocardial and collagenous tissues. As a first approximation, the myocardium was assumed to consist of the non-fibrous and fibrous compartments. The non-fibrous compartment lumps together the normal myocardial constituents including myocytes and supporting cells, and normal interstitial and vascular spaces in a single compartment. The fibrous compartment comprises the total collagen content in the tissue. For fast-exchange, the MRI signal intensity I_j^{fast} for the j^{th} diffusion encoding gradient direction $\boldsymbol{g}_j$ was modeled after a two-compartment MR diffusion equation (43) adapted for DTI,

$$I_j^{fast}=\exp(-b\,\boldsymbol{g}_j^T\cdot[(1-f')\boldsymbol{D}_{myo}+f'\boldsymbol{D}_{col}]\cdot\boldsymbol{g}_j), \quad [1]$$

where $\mathbf{D}_{\text{myo}}$ and $\mathbf{D}_{\text{col}}$ denoted the diffusion tensors for the myocardial (non-fibrous) and collagen compartments, respectively, and b is the scalar diffusion encoding sensitivity. Similarly, the slow-exchange signal equation followed one given previously (44),

$$I_j^{slow}=(1-f')\exp(-b\boldsymbol{g}_j^T\cdot\boldsymbol{D}_{myo}\cdot\boldsymbol{g}_j)+f'\exp(-b\boldsymbol{g}_j^T\cdot\boldsymbol{D}_{col}\cdot\boldsymbol{g}_j)\cdot \quad [2]$$

In both Eq. [1] and [2], the adjusted fractional volume f', given as

$$f'=\frac{f-f_0}{1-f_0}, \quad [3]$$

was used instead of the nominal fractional volume f for the collagen compartment size in order to account for the small but non-negligible level of collagen content f_0 intrinsically found in the normal myocardium.

The mean principal diffusivities determined for the experimental control group in the current study (or D_1, D_2 and D_3 of 0.88, 0.64 and 0.51 x10^{-3} mm^2/s, respectively) were used to construct the diagonal $\mathbf{D}_{\text{myo}}$. The mean collagen content for the same group (7%) was used as f_0. Because DTI parameters for the collagenous compartment were not directly measured in the current study, diffusion properties previously reported (45,46) for collagenous tissues (or 1.2 x10^{-3} mm^2/s each D_1, D_2 and D_3) were used for the diagonal $\mathbf{D}_{\text{col}}$. Due the rather low anisotropy of diffusion in collagenous tissues, with FA reported in the 0.05-0.12 range (46,47), $\mathbf{D}_{\text{col}}$ was assumed to be isotropic.

To avoid the directional dependence of measurement accuracy inherent in each set of encoding gradient directions (41), the diagonal $\mathbf{D}_{\text{myo}}$ was randomly rotated in 3D space and used in Eqs. [1] and [2] to estimate the diffusion signal intensities under simulated but same

experimental conditions (e.g., diffusion encoding directions and b-value) employed in the current study. Moreover, for evaluating the impact of image noise, Gaussian noise comparable to that found in the experimental data (i.e., SNR of 80) was added to the signal intensities, which were then used to compute the scalar DTI parameters, including D_1, D_2, D_3, and FA, of the fibrotic myocardium. In this fashion, DTI parameters under fast and slow compartmental exchange were separately obtained 1000 times and averaged for each level of collagen content (i.e., f) over the range seen in the current study (4% to 32%).

To compare the simulation results to experimental data, the slopes of the simulated DTI profiles (D_1, D_2, D_3, and FA) as a function of collagen content were obtained, and compared to the slope of the linear regression line obtained from the experimental data. Slopes were normalized to units of percentage change per unit of collagen fraction percentage, with the average collagen percentage of the control group taken as the baseline.

Finally, to examine the sensitivity of the choice of f_0 on the estimated diffusivities, the simulations were performed with varying f_0 by 7 ± 1% (i.e., f_0 was set to 6% and 8% in separate runs). The difference between the estimated diffusivities to those obtained from the nominal case $(f_0 = 7\%)$ were calculated and averaged across all simulated collagen fractions for both fast and slow exchange models.

Results

DTI

MR images and DTI-derived FA and MD maps obtained from a representative normal and HF myocardial samples are shown in Fig. 1. Qualitatively, compared to the normal control, lower FA and higher diffusivities were observed in the failing myocardium. The quantified and ROI-averaged values of the DTI parameters for the normal control and HF groups are detailed in Table 2. Consistent with the qualitative observations, the FA in HF specimens was on average 22% lower than normal specimens (0.21 ± 0.01 vs. 0.27 ± 0.02). In contrast, MD of the HF specimens was 12% higher than normal samples (0.76 ± 0.02 vs. 0.68 ± 0.01 × 10^{-3} mm^2/s). Together, the trends of MD and FA suggest that water motility is both higher and less anisotropic in HF than normal myocardial tissues.

The D_1, D_2, and D_3 maps (also shown in Fig. 1) and the corresponding quantified values (Table 2) reveal that the above observed MD and FA changes are results of increases in the tertiary (24% higher in HF, or 0.63 ± 0.02 vs. 0.51 ± 0.02 × 10^{-3} mm^2/s) and secondary diffusivities (14% higher in HF, or 0.73 ± 0.02 vs. 0.64 ± 0.01 × 10^{-3} mm^2/s). The primary diffusivity was not significantly different (0.93 ± 0.02 vs. 0.88 ± 0.02 × 10^{-3} mm^2/s, P = 0.13).

Collagen Evaluation and DTI-Histology Correlation

Representative trichrome sections from control and HF myocardial samples are shown in Fig. 2. Compared to the control specimen (Fig. 2a), the HF slide (Fig. 2b) contains conspicuously higher content of the blue-staining interstitial collagen. Quantitative collagen content measurements are summarized in Table 2. The total collagen content, used as the metric of fibrosis, is nearly 3 times higher in HF than in normal myocardium (19.4 ± 2.0

versus 7.1 ± 1.1 percent area). The level of collagen intrinsic in the normal myocardium is in agreement with the ∼4-5% reported by a previous study (37).

The relationships between different DTI parameters and the total collagen content are shown as scatter plots in Fig. 3. Qualitatively, from the scatter of the data points around the fitted lines, there appears to be more variability in D_1 and FA, compared to D_2 and D_3. The observation is consistent with the Pearson's correlation coefficients between individual DTI parameters and total collagen content, which are listed in Table 3. Among the pairings examined, significant correlations were found between the collagen content (or fibrosis) and FA (r = –0.51), MD (0.59), D_2 (0.56), and D_3 (0.62). The correlation between D_1 and collagen was relatively weaker (r= 0.46), and was not significant (P = 0.05).

Computational Compartmental Analysis

Plots of the Monte Carlo simulated DTI scalar parameters (D_1, D_2, D_3, and FA) vs. collagen percentages are shown in Fig. 4. Overall, simulation results obtained using fast and slow exchange models were in close agreement with experimental data regression line. Both exchange models indicate that all DTI diffusivities would increase, whereas the FA would decrease, as the percent collagen content is increased. Moreover, simulations indicate that the rate of increase as function of collagen content in the secondary and tertiary diffusivities is at least twice as large as that of the primary diffusivity. Specifically, the average collagen content change seen in the current study (Table 2) between normal (baseline) and HF myocardium, 7% to 19%, would correspond to normalized slopes of 0.39, 0.87, and 1.3 for D_1, D_2, and D_3, respectively, and -1.13 for FA (unit of normalized slope is % change per unit of collagen fraction percentage). In comparison, the corresponding quantities from experimental data are 0.51, 0.79, 1.15, and -1.08 for D_1, D_2, D_3, and FA, respectively. Considering the simplifying assumptions used in the exchange models, both the trends as well as the magnitudes of the simulated DTI parameter changes are in strong agreement with the experimental measurements. Finally, the parameter sensitivity analysis suggested that when f_0 was set to 6 or 8%, the estimated diffusivities deviated by 1% compared to the case when f_0 was set to 7%.

Discussion

In this study, DTI was performed on left ventricular specimens obtained from patients with chronic end-stage HF due to idiopathic dilated cardiomyopathy at the time of left ventricular assist device implantation and from normal hearts. Results indicate that HF leads to both significant decrease in the degree of anisotropy (i.e., FA) and significant increase in the water diffusivity (MD, D_2, and D_3) of the myocardium. The trends of the observed changes are consistent with previous DTI studies of myocardial diseases. For example, reduction in the FA and the increase in diffusivities have been reported in studies on myocardial ischemic injury (48,49) and dilated cardiomyopathy (32). Similarly, the FA has been observed to decrease in a DTI study of hypertrophic cardiomyopathy (30). Histological measurements reveal that HF also leads to significant increase in myocardial collagen content (i.e., fibrosis), which is a hallmark of HF (10).

Histological validation of DTI fiber orientation mapping in the myocardium has been extensively reported, in normal hearts (13–15) and, to a lesser extent, disease hearts (32,49). In contrast, few studies have correlated the DTI scalar parameters with histology, and when examined, the correlation was qualitative (32). The present study is the first to demonstrate that scalar DTI parameters are directly correlated to histology, as shown in Table 3 and Fig. 3. Whereas the FA reduction or MD increase associated with HF and their correlation to tissue fibrosis are expected, a noteworthy observation in the current study is that the secondary (D_2) and tertiary (D_3) DTI eigenvalues exhibit a higher correlation with the degree of fibrosis than the primary diffusivity D_1 (r = 0.56 and 0.62, respectively, compared to 0.46). These findings point out a potential role of the indices for characterizing myocardial pathology, and may provide clues to model the effect of fibrosis on the observed DTI signal in the myocardium.

Analysis of the numerical simulations revealed that the behavior of the scalar DTI parameters as a function of the collagen content, including the different sensitivities (i.e., magnitude of the slope) among the diffusivities and FA, can be readily explained by exchange between myocardial and collagen compartments. Moreover, the fact that little difference is seen between simulations using fast and slow exchange models suggests that the behaviors of the scalar DTI parameters largely depend on the mere presence of collagen, with little or no influence from the type of underlying mechanism of compartmental exchange.

The key assumptions made in the numerical compartmental analysis were that the diffusion in the fibrous myocardial compartment is isotropic (i.e., FA = 0), and the intrinsic collagen fraction (f_0) in the normal myocardium in Eq. [3] is 7%. While the first assumption is valid when collagen fibers in the compartment are oriented randomly, or when the collagen is organized but point in a random direction with respect to the myofibers, it would be invalid if the organized collagen follows the same orientation as the myofibers. If the latter had been the case, the simulations would predict the FA of the HF myocardium as a function of collagen content under both fast and slow exchange models to have shallower slopes and deviate away from experimental data points. Consequently, the high degree of agreement between the simulation and empirical results indicate that the assumption of zero FA for the fibrous compartment used in the exchange analysis is valid. Secondly, the parameter sensitivity analysis suggested that the estimated diffusivities obtained from both exchange models are relatively insensitive to the choice of f_0.

Despite the large bulk motion of the heart during the cardiac cycle, in vivo cardiac DTI has been shown both feasible and reproducible in clinical patients (22,23,50–52). Our study paves the way for in vivo clinical trials to evaluate the ability of DTI to assess diffuse fibrosis in vivo. Furthermore, DTI can complement other MRI techniques to characterize myocardial fibrosis in diseased hearts. For example, post contrast T1-mapping has been used as a tool to quantify diffuse fibrosis (53). However, there has been some concern on the use of gadopentate dimeglumine agents in patients with renal failure (54). Hence, it is desirable to explore alternative mechanisms of MRI contrast, especially mechanisms that do not rely on exogenous contrast agents. In this regard, DTI may be an alternative or adjunct method to T1-mapping for detecting and quantifying diffused fibrosis. Even though the observed

correlation between DTI and fibrosis is modest, the strength of correlation was similar to those reported in initial T1 mapping studies (53). Recent advances in T1 mapping studies incorporated modeling of the extracellular volume fraction via relaxation difference between pre- and post-gadolinium contrast administration, which has been shown to improve quantification of diffuse fibrosis (55,56).

In order to improve the accuracy of DTI to quantify diffuse fibrosis, other factors that may affect the DTI measurements have to be taken into account, such as edema, fiber disarray, and age effects. Edema was detected using T2 mapping in patients with dilated cardiomyopathy (57). In a recent study of ischemic reperfusion injury in mice, edema was associated with reduced FA and increased MD (58). Edema was not directly monitored in the current study, and care should be taken in future in vivo DTI studies to rule out the presence of edema. Fiber disarray is another factor that was shown to reduce FA but not MD (30), and therefore has to be accounted for when performing cardiac DTI. Finally, aging hearts were shown to undergo remodeling processes that impact their mechanical and electrical properties (59). Aging hearts were shown to be slightly more fibrotic (with mean fibrosis area being 5% in young vs. 11% in aging hearts) and stiffer when compared to younger hearts (59). Thus, future studies validating DTI to measure diffuse fibrosis should also control for age in the studied population.

There are few other caveats that need to be taken into account in interpreting the results of the current study. First, due to logistical constraints, the sample sizes of the study, 14 for HF and 5 for normal myocardial specimens, are relatively small, which may have prevented some of the observed differences (e.g., D_1) or correlations (D_1 vs. collagen content) from reaching statistical significance. However, the significant differences detected and the smaller variability shown by the DTI parameters compared to histology (as indicated by the SEM values in Table 2) may actually point to a potential advantage of DTI – that DTI can provide rapid and noninvasive assessment for tissue fibrosis with larger spatial coverage than what is currently achievable by histological sectioning. Finally, the current study was conducted on fixed excised specimens, and the findings may or may not be the same as those observed from *in vivo* cardiac DTI. Since both HF and control samples were fixed, regardless of the impact of fixation on the DTI parameters, the differences observed between the groups likely reflected the additional effects introduced by the disease. Moreover, the DTI observations were correlated to histological measurements, which in both the current and other studies were also performed on fixed samples and generally taken to be the gold standard.

In conclusion, the present study suggests that DTI scalar parameters can complement conventional histology and T1-mapping for quantifying diffuse fibrosis. Given the recent technical advances and increasing interest of *in vivo* cardiac DTI (23,50–52), these findings are timely and point to a potential role for DTI in evaluating the tissue collagen content in the nonischemic diseased hearts.

Acknowledgments

This work was supported by National Institutes of Health (NIH) R01 HL092055 and S10 RR023017.

References

1. Roger VL, Go AS, Lloyd-Jones DM, Adams RJ, Berry JD, Brown TM, Carnethon MR, Dai S, de Simone G, Ford ES, Fox CS, Fullerton HJ, Gillespie C, Greenlund KJ, Hailpern SM, Heit Ja, Ho PM, Howard VJ, Kissela BM, Kittner SJ, Lackland DT, Lichtman JH, Lisabeth LD, Makuc DM, Marcus GM, Marelli A, Matchar DB, McDermott MM, Meigs JB, Moy CS, Mozaffarian D, Mussolino ME, Nichol G, Paynter NP, Rosamond WD, Sorlie PD, Stafford RS, Turan TN, Turner MB, Wong ND, Wylie-Rosett J. Heart disease and stroke statistics--2011 update: a report from the American HeartAssociation. Circulation. 2011; 123(4):e18–e209. [PubMed: 21160056]
2. Dickstein K, Cohen-Solal A, Filippatos G, McMurray JJV, Ponikowski P, Poole-Wilson PA, Strömberg A, van Veldhuisen DJ, Atar D, Hoes AW, Keren A, Mebazaa A, Nieminen M, Priori SG, Swedberg K, Vahanian A, Camm J, De Caterina R, Dean V, Funck-Brentano C, Hellemans I, Kristensen SD, McGregor K, Sechtem U, Silber S, Tendera M, Widimsky P, Zamorano JL, Auricchio A, Bax J, Böhm M, Corrà U, Della Bella P, Elliott PM, Follath F, Gheorghiade M, Hasin Y, Hernborg A, Jaarsma T, Komajda M, Kornowski R, Piepoli M, Prendergast B, Tavazzi L, Vachiery JL, Verheugt FWa, Zannad F. ESC guidelines for the diagnosis and treatment of acute and chronic heart failure 2008. Eur Heart J. 2008; 29(19):2388–442. [PubMed: 18799522]
3. Mann DL, Bristow MR. Mechanisms and models in heart failure: the biomechanical model and beyond. Circulation. 2005; 111(21):2837–49. [PubMed: 15927992]
4. Tamaki S, Mano T, Sakata Y, Ohtani T, Takeda Y, Kamimura D, Omori Y, Tsukamoto Y, Ikeya Y, Kawai M, Kumanogoh A, Hagihara K, Ishii R, Higashimori M, Kaneko M, Hasuwa H, Miwa T, Yamamoto K, Komuro I. Interleukin-16 promotes cardiac fibrosis and myocardial stiffening in heart failure with preserved ejection fraction. PLoS One. 2013; 8(7):e68893. [PubMed: 23894370]
5. Ten Tusscher KHWJ, Panfilov AV. Influence of diffuse fibrosis on wave propagation in human ventricular tissue. Europace. 2007; Suppl 6(9):vi38–45. [PubMed: 17959692]
6. Bohl, S.; Schulz-Menger, J. Heart, lung & circulation. Australasian Society of Cardiac and Thoracic Surgeons and The Cardiac Society of Australia and New Zealand; 2010. Cardiovascular magnetic resonance imaging of non-ischaemic heart disease: establishedand emerging applications. [Internet].
7. Jellis, C.; Martin, J.; Narula, J.; Marwick, TH. J Am Coll Cardiol. Vol. 56. Elsevier Inc.; 2010. Assessment of nonischemic myocardial fibrosis; p. 89-97.
8. Weber KT, Brilla CG. Pathological hypertrophy and cardiac interstitium. Fibrosis and renin-angiotensin-aldosterone system. Circulation. 1991; 83(6):1849–65. [PubMed: 1828192]
9. Beltrami, Ca; Finato, N.; Rocco, M.; Feruglio, Ga; Puricelli, C.; Cigola, E.; Quaini, F.; Sonnenblick, EH.; Olivetti, G.; Anversa, P. Structural basis of end-stage failure in ischemic cardiomyopathy in humans. Circulation. 1994; 89(1):151–63. [PubMed: 8281642]
10. Drakos SG, Kfoury AG, Stehlik J, Selzman CH, Reid BB, Terrovitis JV, Nanas JN, Li DY. Bridge to recovery: understanding the disconnect between clinical and biological outcomes. Circulation. 2012; 126(2):230–41. [PubMed: 22777666]
11. Diez J. Losartan-Dependent Regression of Myocardial Fibrosis Is Associated With Reduction of Left Ventricular Chamber Stiffness in Hypertensive Patients. Circulation. 2002; 105(21):2512–7. [PubMed: 12034658]
12. Basser PJ, Mattiello J, LeBihan D. MR diffusion tensor spectroscopy and imaging. Biophys J. 1994; 66(1):259–67. [PubMed: 8130344]
13. Hsu EW, Muzikant AL, Matulevicius SA, Penland RC, Henriquez CS. Magnetic resonance myocardial fiber-orientation mapping with direct histological correlation. Am J Physiol Hear Circ Physiol. 1998; 274(5 Pt 2):H1627–34.
14. Scollan DF, Holmes A, Winslow R, Forder J. Histological validation of myocardial microstructure obtained from diffusion tensor magnetic resonance imaging. Am J Physiol Hear Circ Physiol. 1998; 275(6 Pt 2):H2308–18.
15. Holmes A, Scollan DF, Winslow RL. Direct histological validation of diffusion tensor MRI in formaldehyde-fixed myocardium. Magn Reson Med. 2000; 44(1):157–61. [PubMed: 10893534]
16. Tseng WYI, Wedeen VJ, Reese TG, Smith RN, Halpern EF. Diffusion tensor MRI of myocardial fibers and sheets: correspondence with visible cut-face texture. J Magn Reson Imaging. 2003; 17(1):31–42. [PubMed: 12500272]

17. Jiang Y, Pandya K, Smithies O, Hsu EW. Three-dimensional diffusion tensor microscopy of fixed mouse hearts. Magn Reson Med. 2004; 52(3):453–60. [PubMed: 15334561]
18. Jiang Y, Guccione JM, Ratcliffe MB, Hsu EW. Transmural heterogeneity of diffusion anisotropy in the sheep myocardium characterized by MR diffusion tensor imaging. Am J Physiol Hear Circ Physiol. 2007; 293(4):H2377–84.
19. Healy LJ, Jiang Y, Hsu EW. Quantitative comparison of myocardial fiber structure between mice, rabbit, and sheep using diffusion tensor cardiovascular magnetic resonance. J Cardiovasc Magn Reson. 2011; 13:74. [PubMed: 22117695]
20. Geerts L, Bovendeerd P, Nicolay K, Arts T. Characterization of the normal cardiac myofiber field in goat measured with MR-diffusion tensor imaging. Am J Physiol Heart Circ Physiol. 2002; 283(1):H139–45. [PubMed: 12063284]
21. Chen J, Liu W, Zhang H, Lacy L, Yang X, Song SK, Wickline Sa, Yu X. Regional ventricular wall thickening reflects changes in cardiac fiber and sheetstructure during contraction: quantification with diffusion tensor MRI. Am J Physiol Hear Circ Physiol. 2005; 289(5):H1898–907.
22. Reese TG, Weisskoff RM, Smith RN, Rosen BR, Dinsmore RE, Wedeen VJ. Imaging myocardial fiber architecture in vivo with magnetic resonance. Magn Reson Med. 1995; 34(6):786–91. [PubMed: 8598805]
23. Dou J, Reese TG, Tseng WYI, Wedeen VJ. Cardiac diffusion MRI without motion effects. Magn Reson Med. 2002; 48(1):105–14. [PubMed: 12111937]
24. Wu M, Tseng W-YI, Su MM, Liu C, Chiou KR, Wedeen VJ, Reese TG, Yang CF. Diffusion tensor magnetic resonance imaging mapping the fiber architecture remodeling in human myocardium after infarction: correlation with viability and wall motion. Circulation. 2006; 114(10):1036–45. [PubMed: 16940196]
25. Wu MT, Su MYM, Huang YL, Chiou KR, Yang P, Pan HB, Reese TG, Wedeen VJ, Tseng WYI. Sequential changes of myocardial microstructure in patients postmyocardial infarction by diffusion-tensor cardiac MR: correlation with left ventricular structure and function. Circ Cardiovasc Imaging. 2009; 2(1):32–40. [PubMed: 19808562]
26. Chen J, Song SK, Liu W, McLean M, Allen JS, Tan J, Wickline Sa, Yu X. Remodeling of cardiac fiber structure after infarction in rats quantified withdiffusion tensor MRI. Am J Physiol Hear Circ Physiol. 2003; 285(3):H946–54.
27. Wu Y, Wu EX. MR investigation of the coupling between myocardial fiber architecture and cardiac contraction. Conf Proc IEEE Eng Med Biol Soc. 2009; 2009:4395–8. [PubMed: 19964360]
28. Pop M, Ghugre NR, Ramanan V, Morikawa L, Stanisz G, Dick AJ, Wright Ga. Quantification of fibrosis in infarcted swine hearts by ex vivo lategadolinium-enhancement and diffusion-weighted MRI methods. Phys Med Biol. 2013; 58(15):5009–28. [PubMed: 23833042]
29. Helm PA, Younes L, Beg MF, Ennis DB, Leclercq C, Faris OP, McVeigh E, Kass D, Miller MI, Winslow RL. Evidence of structural remodeling in the dyssynchronous failing heart. Circ Res. 2006; 98(1):125–32. [PubMed: 16339482]
30. Tseng WYI, Dou J, Reese TG, Wedeen VJ. Imaging myocardial fiber disarray and intramural strain hypokinesis in hypertrophic cardiomyopathy with MRI. J Magn Reson Imaging. 2006; 23(1):1–8. [PubMed: 16331592]
31. Eggen MD, Swingen CM, Iaizzo PA. Analysis of fiber orientation in normal and failing human hearts using diffusion tensor MRI. EEE International Symposium on Biomedical Imaging: From Nano to Macro. Ieee. 2009:642–5.
32. Li W, Lu M, Banerjee S, Zhong J, Ye A, Molter J, Yu X. Ex vivo diffusion tensor MRI reflects microscopic structural remodeling associated with aging and disease progression in normal and cardiomyopathic Syrian hamsters. NMR Biomed. 2009; 22(8):819–25. [PubMed: 19434665]
33. McConnell HM. Reaction Rates by Nuclear Magnetic Resonance. J Chem Phys. 1958; 28(3):430.
34. Kärger J. NMR self-diffusion studies in heterogeneous systems. Adv Colloid Interface Sci. 1985; 23(0):129–48.
35. Forder JR, Bui JD, Buckley DL, Blackband SJ. MR imaging measurement of compartmental water diffusion in perfused heart slices. Am J Physiol Hear Circ Physiol. 2001; 281:H1280–H1285.

36. Hsu EW, Buckley DL, Bui JD, Blackband SJ, Forder JR. Two-component diffusion tensor MRI of isolated perfused hearts. Magn Reson Med. 2001; 45(6):1039–45. [PubMed: 11378882]
37. Drakos SG, Kfoury AG, Hammond EH, Reid BB, Revelo MP, Rasmusson BY, Whitehead KJ, Salama ME, Selzman CH, Stehlik J, Clayson SE, Bristow MR, Renlund DG, Li DY. Impact of mechanical unloading on microvasculature and associated central remodeling features of the failing human heart. J Am Coll Cardiol. 2010; 56(5):382–91. [PubMed: 20650360]
38. Kim TH, Zollinger L, Shi XF, Rose J, Jeong EK. Diffusion tensor imaging of ex vivo cervical spinal cord specimens: the immediate and long-term effects of fixation on diffusivity. Anat Rec. 2009; 292(2):234–41.
39. Watson, B.; Hsu, E. Effects of Formalin Fixation on Diffusion Tensor Imaging of Myocardial Tissues. ISMRM 20th Annual Meeting; 2012.
40. Unverferth DV, Fetters JK, Unverferth BJ, Leier CV, Magorien RD, Arn aR, Baker PB. Human myocardial histologic characteristics in congestive heart failure. Circulation. 1983; 68(6):1194–200. [PubMed: 6640872]
41. Papadakis NG, Xing D, Huang CL, Hall LD, Carpenter Ta. A comparative study of acquisition schemes for diffusion tensor imaging using MRI. J Magn Reson. 1999; 137(1):67–82. [PubMed: 10053134]
42. Le Bihan D, Mangin JF, Poupon C, Clark Ca, Pappata S, Molko N, Chabriat H. Diffusion tensor imaging: concepts and applications. J Magn Reson Imaging. 2001; 13(4):534–46. [PubMed: 11276097]
43. Niendorf T, Dijkhuizen RM, Norris DG, van Lookeren Campagne M, Nicolay K. Biexponential diffusion attenuation in various states of brain tissue: implications for diffusion-weighted imaging. Magn Reson Med. 1996; 36(6):847–57. [PubMed: 8946350]
44. Hsu EW, Buckley DL, Bui JD, Blackband SJ, Forder JR. Two-component diffusion tensor MRI of isolated perfused hearts. Magn Reson Med. 2001; 45(6):1039–45. [PubMed: 11378882]
45. Henkelman RM, Stanisz GJ, Kim JK, Bronskill MJ. Anisotropy of NMR properties of tissues. Magn Reson Med. 1994; 32(5):592–601. [PubMed: 7808260]
46. Hsu EW, Setton LA. Diffusion tensor microscopy of the intervertebral disc anulus fibrosus. Magn Reson Med. 1999; 41(5):992–9. [PubMed: 10332883]
47. De Visser SK, Bowden JC, Wentrup-Byrne E, Rintoul L, Bostrom T, Pope JM, Momot KI. Anisotropy of collagen fibre alignment in bovine cartilage: comparison of polarised light microscopy and spatially resolved diffusion-tensor measurements. Osteoarthritis Cartilage. 2008; 16(6):689–97. [PubMed: 18023211]
48. Wu EX, Wu Y, Nicholls JM, Wang J, Liao S, Zhu S, Lau CP, Tse HF. MR diffusion tensor imaging study of postinfarct myocardium structural remodeling in a porcine model. Magn Reson Med. 2007; 58(4):687–95. [PubMed: 17899595]
49. Chen J, Song SK, Liu W, McLean M, Allen JS, Tan J, Wickline Sa, Yu X. Remodeling of cardiac fiber structure after infarction in rats quantified withdiffusion tensor MRI. Am J Physiol Hear Circ Physiol. 2003; 285(3):H946–54.
50. Gamper U, Boesiger P, Kozerke S. Diffusion imaging of the in vivo heart using spin echoes-considerations on bulk motion sensitivity. Magn Reson Med. 2007; 57(2):331–7. [PubMed: 17260376]
51. McGill LA, Ismail TF, Nielles-Vallespin S, Ferreira P, Scott AD, Roughton M, Kilner PJ, Ho SY, McCarthy KP, Gatehouse PD, de Silva R, Speier P, Feiweier T, Mekkaoui C, Sosnovik DE, Prasad SK, Firmin DN, Pennell DJ. Reproducibility of in-vivo diffusion tensor cardiovascular magnetic resonance in hypertrophic cardiomyopathy. J Cardiovasc Magn Reson. 2012; 14(1):86. [PubMed: 23259835]
52. Nielles-Vallespin S, Mekkaoui C, Gatehouse P, Reese TG, Keegan J, Ferreira PF, Collins S, Speier P, Feiweier T, de Silva R, Jackowski MP, Pennell DJ, Sosnovik DE, Firmin D. In vivo diffusion tensor MRI of the human heart: Reproducibility of breath-hold and navigator-based approaches. Magn Reson Med. 2012
53. Iles L, Pfluger H, Phrommintikul A, Cherayath J, Aksit P, Gupta SN, Kaye DM, Taylor AJ. Evaluation of diffuse myocardial fibrosis in heart failure with cardiac magnetic resonance contrast-enhanced T1 mapping. J Am Coll Cardiol. 2008; 52(19):1574–80. [PubMed: 19007595]

54. Marckmann P, Skov L, Rossen K, Dupont A, Damholt MB, Heaf JG, Thomsen HS. Nephrogenic systemic fibrosis: suspected causative role of gadodiamide used for contrast-enhanced magnetic resonance imaging. J Am Soc Nephrol. 2006; 17(9):2359–62. [PubMed: 16885403]

55. Messroghli D, Nordmeyer S, Dietrich T, Dirsch O, Kaschina E, Savvatis K, O H-Ici D, Klein C, Berger F, Kuehne T. Assessment of Diffuse Myocardial Fibrosis in Rats Using Small Animal Look-Locker Inversion Recovery (SALLI) T1 Mapping. Circ Cardiovasc Imaging. 2011; 4(6): 636–40. [PubMed: 21917782]

56. Flett AS, Hayward MP, Ashworth MT, Hansen MS, Taylor AM, Elliott PM, McGregor C, Moon JC. Equilibrium contrast cardiovascular magnetic resonance for the measurement of diffuse myocardial fibrosis: preliminary validation in humans. Circulation. 2010; 122(2):138–44. [PubMed: 20585010]

57. Nishii, T.; Kono, A.; Shigeru, M.; Takamine, S.; Fujiwara, S.; Kyotani, K.; Aoyama, N.; Sugimura, K. Int J Cardiovasc Imaging. Springer Netherlands; 2014. Cardiovascular magnetic resonance T2 mapping can detect myocardial edema in idiopathic dilated cardiomyopathy; p. 1-8.

58. Sosnovik DE, Mekkaoui C, Huang S, Chen HH, Dai G, Stoeck CT, Ngoy S, Guan J, Wang R, Kostis WJ, Jackowski MP, Wedeen VJ, Kozerke S, Liao R. Microstructural Impact of Ischemia and Bone Marrow-Derived Cell Therapy Revealed with Diffusion Tensor MRI Tractography of the Heart In Vivo. Circulation. 2014; 129(17):1731–41. [PubMed: 24619466]

59. Cooper LL, Odening KE, Hwang MS, Chaves L, Schofield L, Taylor Ca, Gemignani AS, Mitchell GF, Forder JR, Choi BR, Koren G. Electromechanical and structural alterations in the aging rabbit heart and aorta. Am J Physiol Heart Circ Physiol. 2012; 302(8):H1625–35. [PubMed: 22307668]

List of Abbreviation

DTI	Diffusion tensor imaging
HF	heart failure
FA	fractional anisotropy
MD	mean diffusivity
LVAD	left ventricular assist device
NYHA	New York Heart Association

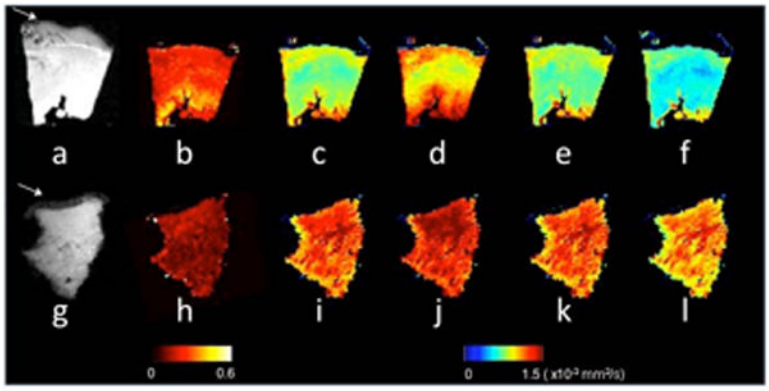

Figure 1.

Representative DTI scalar maps from control and failing heart cores. The top panel shows a MR image without diffusion weighting (B0), FA, MD, D_1, D_2, and D_3 maps for normal (a-f), whereas the lower panel shows the failing core (g-l). A transverse view is shown, with the endocardium located at the top. The pericardial fat visible in the B0 image (white arrows in a and g) was segmented out in the DTI processing step. The DTI parameters are shown in falsecolor according to the colorbars, and all diffusivities had the same color scaling with units of 10^{-3} mm^2/s.

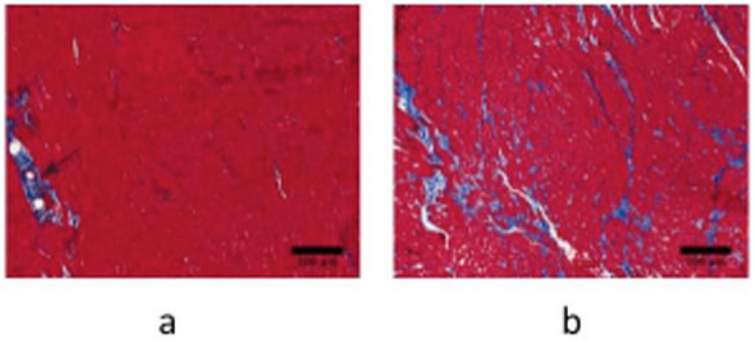

Figure 2.

Histological evaluation of control and failing heart cores. Masson's trichrome histological images of collagen content (20x magnification, collagen stains in blue) from a representative control (a) and failing (b) heart cores. The black arrow in (a) points to perivascular collagen, which was included as part of the total collagen calculation reported in this study.

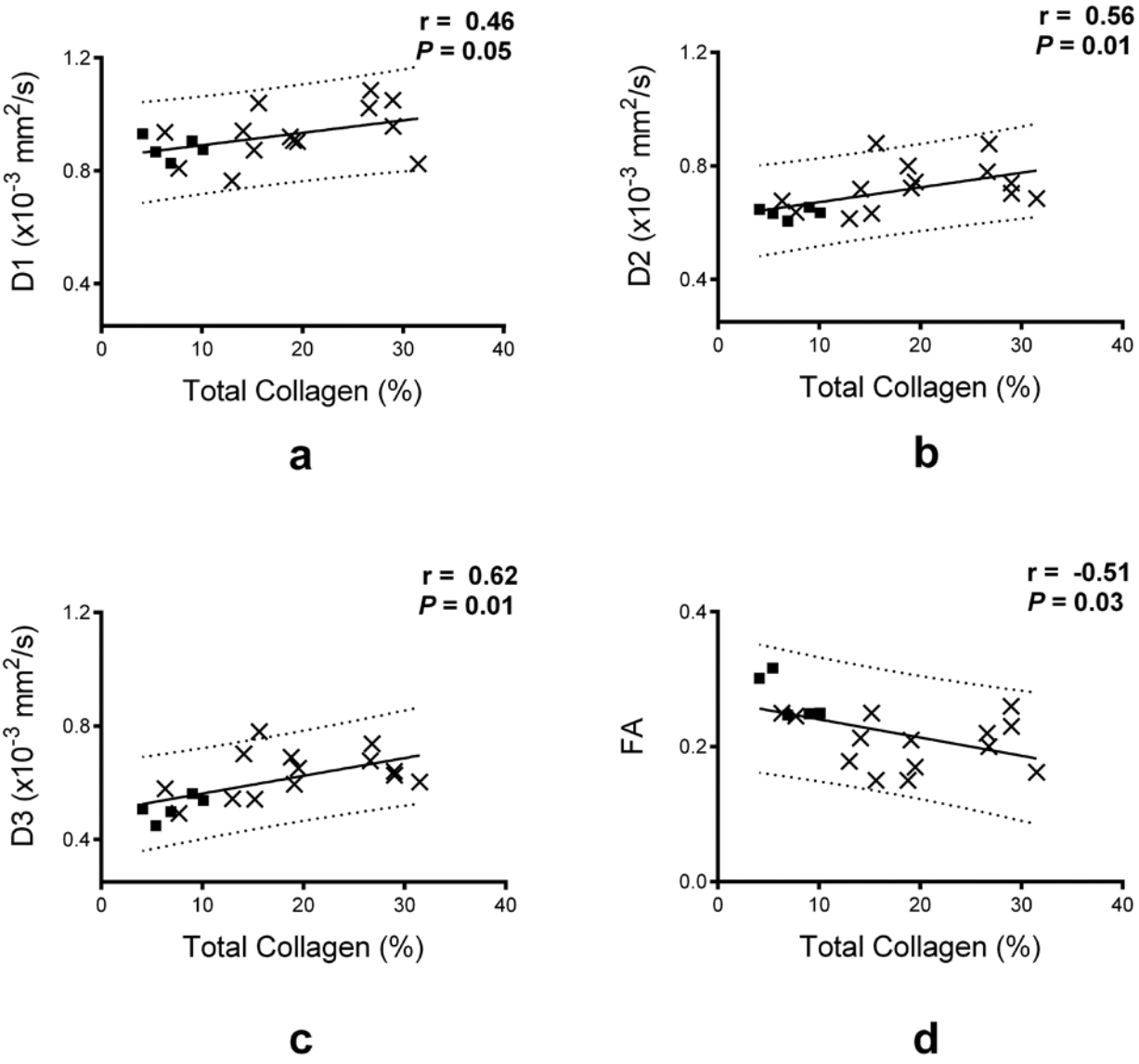

Figure 3.

Quantitative correlation between DTI scalar parameters and collagen content. Scatter plots of FA, D_1, D_2 and D_3 as a function of collagen content are shown with the experimental data (displayed as solid squares for the control group, and as x for the failing group) and the linear regression fit (solid black line) and the 95% prediction interval (dashed lines). The linear regression coefficient (r) and its corresponding *P* value are reported with each plot.

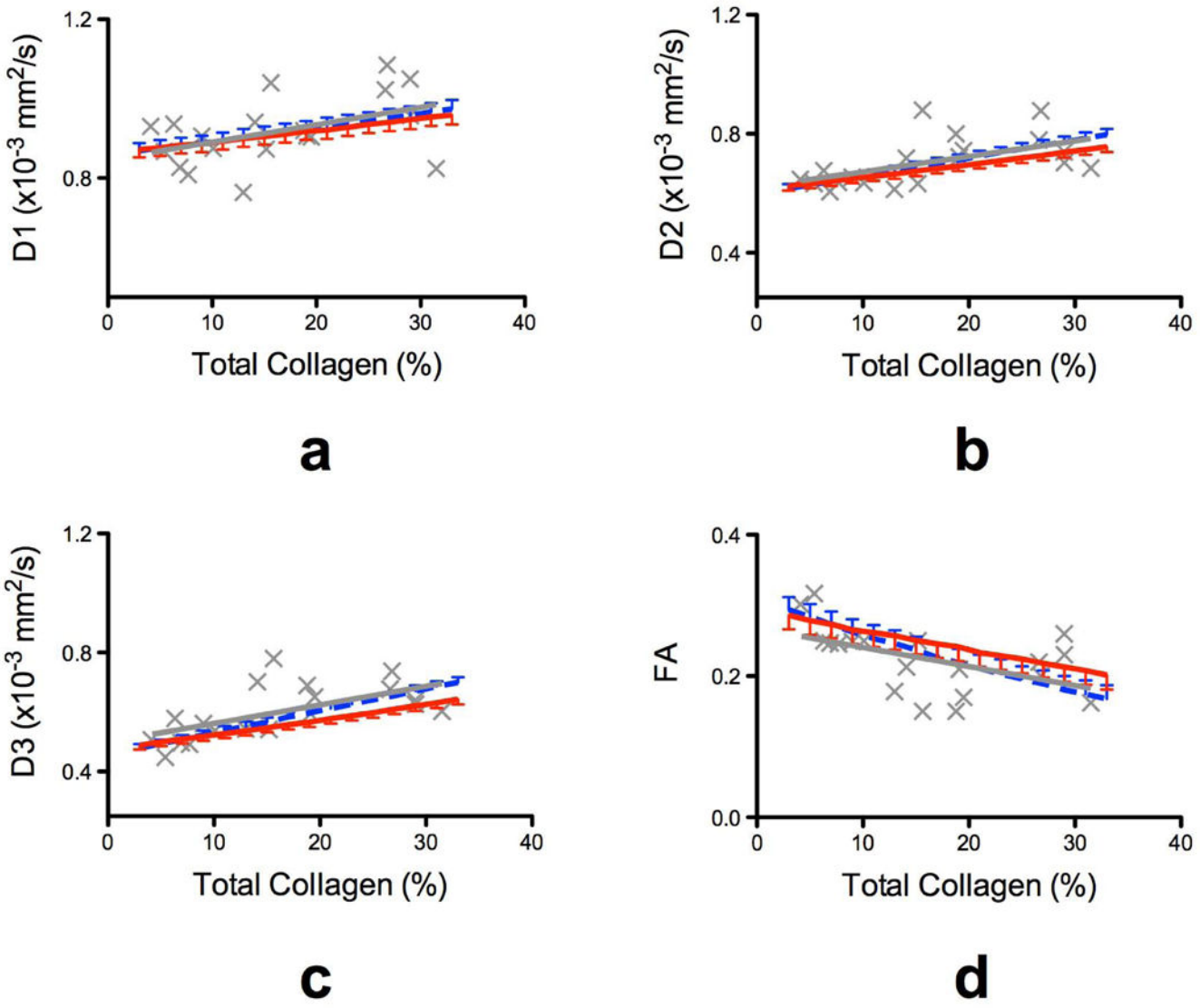

Figure 4.

Monte Carlo computer simulation of DTI scalar parameters as function of collagen content (%). The standard DTI measurements were simulated when the underlying diffusion signal was assumed to originate from either fast (dotted blue line, with upper standard deviation error bars) or slow (solid red line with lower standard deviation error bars) exchange between the two compartments. The experimental data and their regression fit line are overlaid on each plot in gray (x for individual measurements, and solid gray line for the linear regression fit). Little difference was seen between fast and slow exchange model predictions compared to the variability observed in the experimental data.

Table 1

Baseline characteristics of the 14 patients with chronic HF due to idiopathic dilatedcardiomyopathy, and 5 normal donors. ICMP (ischemic cardiomyopathy), NYHA (New York Heart Association), LVEF (left ventricle ejection fraction), LVEDD (left ventricular end-diastolic diameter), LVESD (left ventricular end-systolic diameter), RAP (right atrial pressure), PASP (systolic pulmonary artery pressure), MPAP (mean pulmonary artery pressure), PCWP (pulmonary capillary wedge pressure), PVR (pulmonary vascular resistance), CI (cardiac index), BUN (blood urea nitrogen).

Parameter	HF Patients (N=14)	Normal Donor (N=5)
Age, years	52 ± 14.8	21 ± 3.6
Male gender	84%	60%
HF etiology		
IDC	100%	n/a
ICMP	0%	n/a
NYHA class		
II	6%	n/a
III	47%	n/a
IV	47%	n/a
LVEF, %	16 ± 6.1	62 ± 6
LVEDD, cm	6.8 ± 0.99	4.1 ± 0.41
LVESD, cm	6.2 ± 1.0	2.7 ± 0.32
RAP, mm Hg	12 ± 5.9	7 ± 3.1
PASP, mmHg	49 ±13.5	-
MPAP, mm Hg	34 ± 9.9	-
PCWP, mm Hg	22 ± 10.0	7.2 ± 1.6
PVR, Woods units	4.1 ± 3.2	-
CI, LPM/m^2	1.8 ± 0.7	3.5 ± 0.5
Hemoglobin, g/dl	13 ± 1.5	13.9 ± 1.3
Sodium, mEq/L	136 ± 3.2	139 ± 2.1
BUN, mg/dl	24 ± 7.7	14.2 ± 5.8
Creatinine, mg/dl	1.21 ± 0.4	1.1 ± 0.1
Total bilirubin, mg/dl	1.31 ± 0.7	0.32 ± 0.23

Table 2

DTI and quantitative collagen measurements obtained from control and failing hearts. FA (fractional anisotropy), MD (mean diffusivity), D_1 (primary diffusivity), D_2 (secondary diffusivity), and D_3 (tertiary diffusivity). DTI and collagen measurements were obtained from ROIs covering the whole imaged tissue area.

	FA	MD 10^{-3} mm^2/s	D_1 10^{-3} mm^2/s	D_2 10^{-3} mm^2/s	D_3 10^{-3} mm^2/s	Collagen (%)
Control (n=5)	0.27±0.02	0.68±0.01	0.88±0.02	0.64±0.01	0.51±0.02	7.1±1.1
Failing (n=14)	0.21±0.01	0.76±0.02	0.93±0.02	0.73±0.02	0.63±0.02	19.4±2.0
***P*-value**	<0.01	<0.01	0.13	<0.01	<0.01	<0.01

Table 3

Pearson's correlation coefficient (r) and *P*-values between DTI scalar parameters and total collagen. FA (fractional anisotropy), MD (mean diffusivity), D1 (primary diffusivity), D2 (secondary diffusivity), D3 (tertiary diffusivity).

	FA	**MD**	**D_1**	**D_2**	**D_3**
$r-\text{value}$	− 0.51	0.59	0.46	0.56	0.62
P-value	<0.05	<0.02	0.05	<0.02	<0.01